Chapter 5

MOKE in the Soft-X-Ray Region (XMOKE)

The interest in MOKE in the soft-x-ray region arises from the strong amplification of the light scattering cross section and magnetic contrast at the absorption edges (compared to MOKE with visible light) and the resulting relatively short penetration depth which is the basis for element specific MOKE. In section 5.1 measurements of the specularly reflected light intensity at the $N_{4,5}$ and $M_{4,5}$ absorption thresholds of Tb and Gd are presented. Due to the strong magnetic contrast, i.e. magnetization dependent difference in absorption, a reorientation of the magnetization involves strong changes in penetration depth. Effects that affect the proportionality between XMOKE signal and magnetization, originating from the crystalline magnetic structure or the photon energy selection, are discussed in section 5.2. The knowledge of the optical constants β and δ enables one to calculate the expected contributions from film and substrate to the total reflected light intensity and therefore give a quantitative estimation of interference effects in the MOKE signal. As an example the optical constants of Gd at the $N_{4,5}$ threshold, determined on the basis of absorption measurements are presented in section 5.3. Finally calculated reflection spectra (Fresnel equations) for either magnetization are presented in section 5.4.

5.1 Lanthanide $N_{4,5}$ and $M_{4,5}$ absorption thresholds

The first example of a simple lanthanide system is an in-plane magnetized 8 nm thick gadolinium (Gd) metal film grown *in situ* by metal vapor deposition on a single-crystal W(110) substrate [117]. Fig. 5.1(a) shows two Gd $4d-4f$ absorption spectra, with the film magnetized either parallel (dotted) or antiparallel (solid curve) to the projected direction of a beam of circularly polarized (CP) synchrotron radiation [160]. Upon magnetization reversal the weak pre-edge absorption lines change strongly, and the broad absorption maximum near $h\nu = 149$ eV apparently shifts by over 1 eV [161]. The associated pair of x-ray reflectivity spectra is presented in Fig. 5.1(b), recorded from the same film by using a photodiode in specular geometry (see inset). For both magnetization directions there is

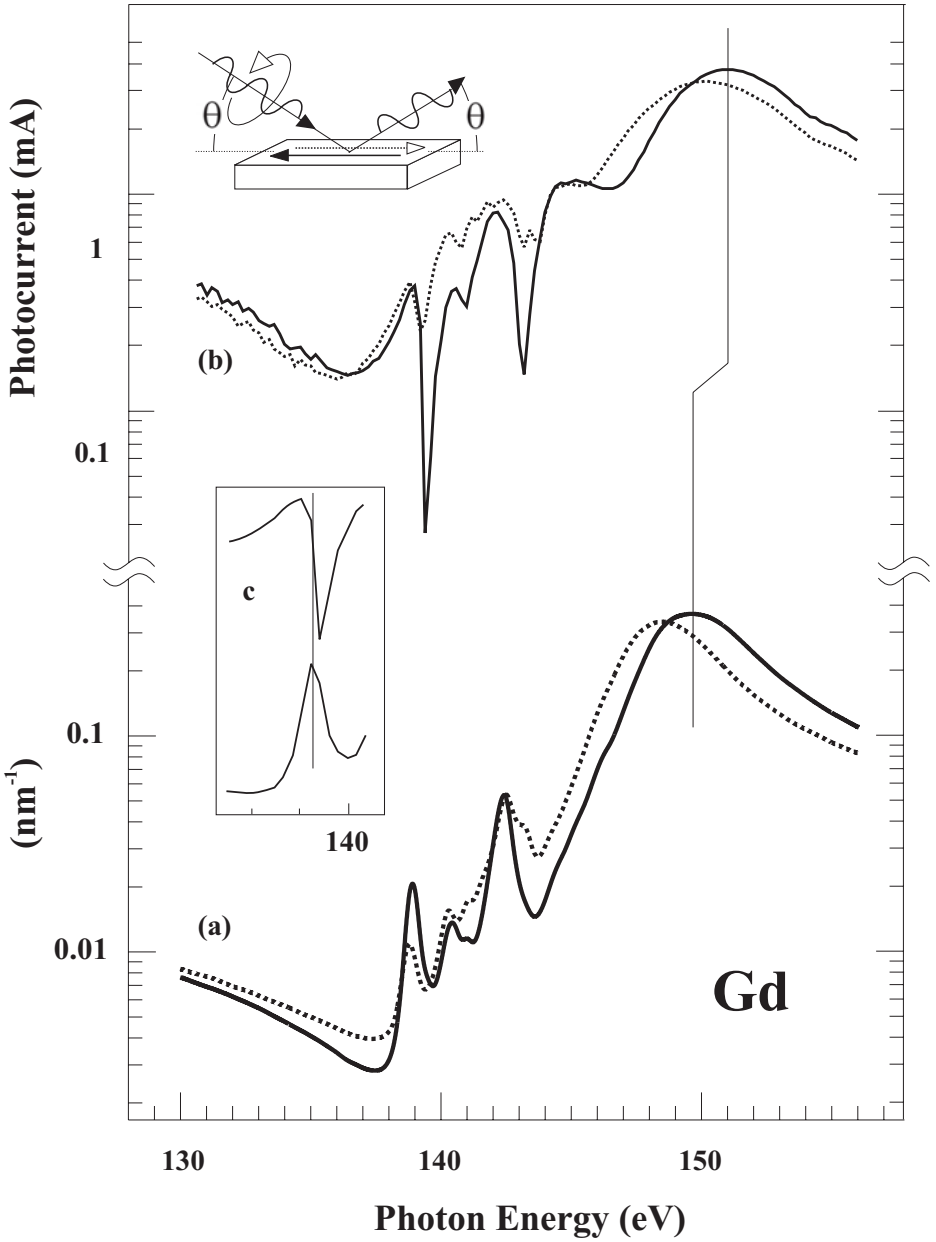

Figure 5.1. Comparison of reflection (a) and absorption (b) spectra of a thick gadolinium film (d=8nm) at the $N_{4,5}$-edge. (c) For the nearly isolated pre-edge line at lowest excitation energy the absorption maximum is found to coincide with the point of steepest descent of the reflectivity structure; it is obviously dominated by the dispersive part of the refractive index. (Measured at the undulator beamline UE56-1, BESSY.)

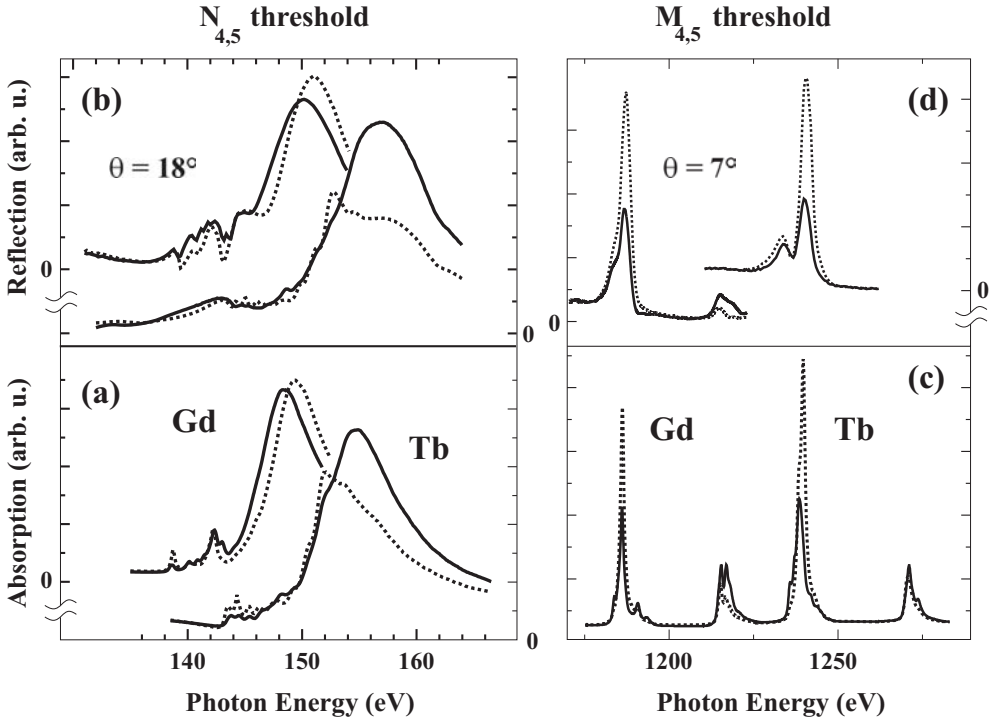

Figure 5.2. Magnetic circular dichroism spectra in (a,c) absorption and in (b,d) reflection of remanently magnetized Gd and Tb films at low temperature ($\sim$ 30 K). While the $N_{4,5}$ spectral ranges of Gd and Tb overlap, element specifity is obtained at the $M_{4,5}$ edges. The absorption spectra (a,c) were recorded at $\theta = 30°$ grazing incidence angle by total electron yield.

a pronounced maximum of 20 times higher reflected intensity compared to the minimum near 136 eV. The reflectivity maxima (solid and dotted curves) are located $\sim$ 1.5 eV above the corresponding giant absorption peaks (Fig. 5.1(a)). In the pre-edge region only dispersive-like structures appear in reflectivity with the points of steepest slope coinciding with the associated absorption peaks (most evident for the lowest energy line magnified in Fig. 5.1(c)). These features are readily understood within elementary dispersion theory which formally describes the interaction of light with metals by introduction of a complex refractive index, $n = 1 - \delta + i\beta$, and assuming that electrons are bound by elastic forces with oscillator energies equal to the optical transition energies [162].

While for light in normal incidence both the absorptive part k and the dispersive part δ contribute equally to the reflected intensity, the dispersive part clearly dominates at grazing incidence according to the Fresnel formulae [162]. The obvious difference in reflectivity line shape between pre-edge and Giant region (Fig. 5.1(b)) is simply due to the different transition probabilities (line strengths) in the two energy regions. The reflected light intensity at some constant grazing angle θ (cf. inset of Fig. 5.1(b)) scales with the electric-dipole transition probability. It has the general property (Wigner-Eckart theorem) that for CP-light excitation in magnetically ordered media the difference in transition probability for oppositely magnetized samples (+ or -) is proportional to the magnetization [48].

Consequently the difference of $4d-4f$ specularly reflected intensity is proportional to the 4f-shell magnetization [39],

$$R_\Theta^+ - R_\Theta^- \propto \mid M_{4f} \mid \ . \tag{5.1}$$

This simple relation holds strictly when all light is absorbed, i.e. for semi-infinite samples. However, owing to the particularly short attenuation length l_{abs} near the lanthanide $4d-4f$ giant absorption maxima, Eq. (1) is approximately valid also for thin films and simple layered structures of lanthanide elements as long as the thickness d of the layer containing the absorbing element clearly exceeds l_{abs}. This is principally different from $2p-3d$ transitions in transition metals where attenuation lengths of ∼20 nm usually cause substantial interference in structures of nanometer size which inhibits the straight-forward interpretation in terms of sample magnetization [20].

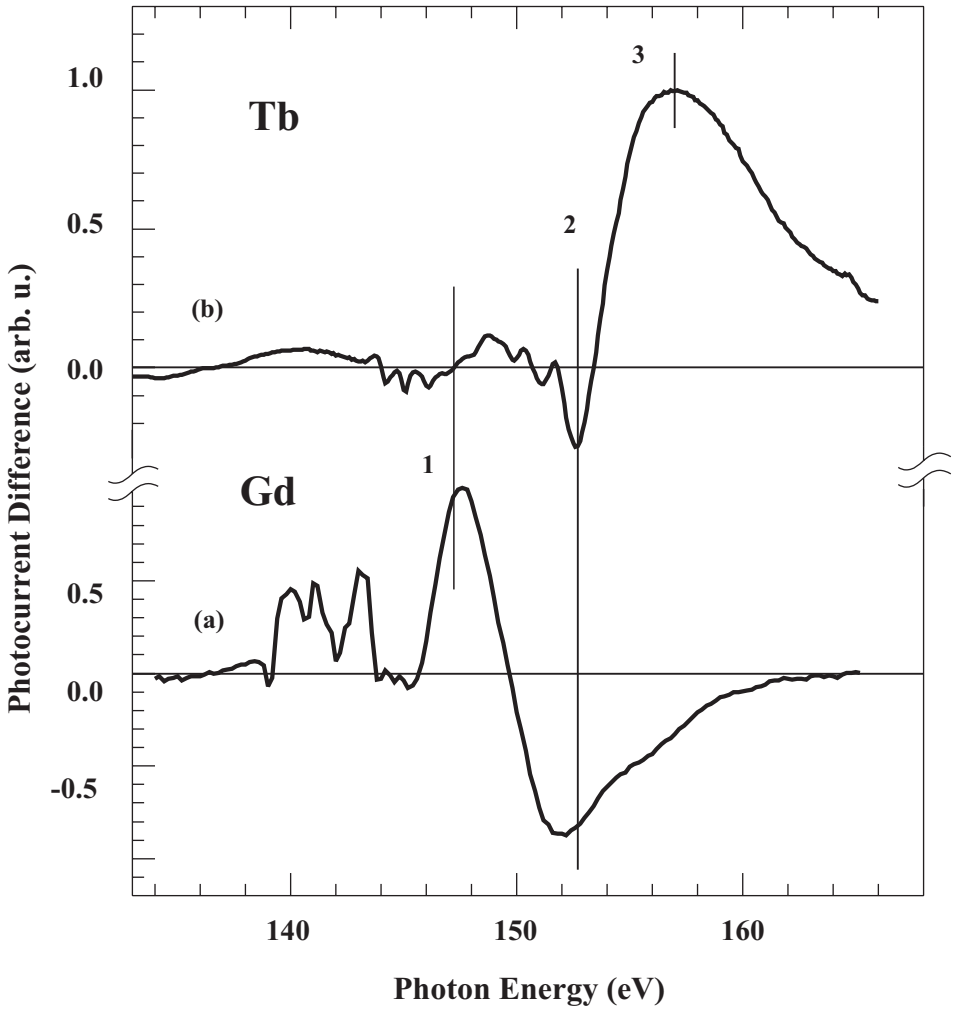

Figure 5.3. Magnetic contrast for (a) Gd and (b) Tb is obtained from the difference in reflection upon reversal of the magnetization. Notice that the signal is in the order of μA !

Unlike MO transitions in the visible-light region [1,163] the energy at which the $4d-4f$

transition occurs changes significantly in going across the lanthanide series, so that even neighbors in the periodic table can easily be distinguished. An overview of magnetic circular dichroism spectra of magnetized Gd and Tb metal films is given in Fig. 5.2. The left panel presents spectra taken at the $N_{4,5}(4d-4f)$ thresholds in (a) absorption and (b) reflection. The spectra were taken at remanent in-plane magnetization with the magnetization either parallel (solid curves) or antiparallel (dotted curves) to the surface-projected photon spin of the incident circularly polarized x-ray beam. Obviously large magnetic dichroic effects are observed in both, absorption and reflection, as expected since absorptive part (β) and dispersive part (δ) of the complex refractive index are correlated (Kramers-Kronig [43]).

The giant resonance spectra of Gd and Tb at the $N_{4,5}$ thresholds of the two elements overlap to some extent which leads to non-perfect element specificity in this case. In Fig. 5.3 the difference between spin-up and spin-down in the reflectivity spectra of (a) Gd and (b) Tb are compared. The Tb MO signal peaks near the Tb Giant absorption at hv = 157 eV which is several eV above the region of substantial MO signal from Gd. Large magnetic dichroic effects are observed both in the pre-edge regions with relatively narrow absorption lines and in the giant-resonance regions. At the maximum of the giant resonance the attenuation length l_{abs} is only of the order of a few nanometers (cf. Table 5.1) compared to $\sim$ 100 nm in the pre-edge region [34, 42]. The analogous spectra at the $M_{4,5}$ thresholds involving the deeper $3d$ core electrons are presented in the right panel of Fig. 5.2(c) for absorption and (d) for reflection. In this case, the 3d spin-orbit interaction is substantially larger than the 3d/4f-multiplett splitting which leads to a complete separation of the absorption spectra of Gd and Tb, i.e. to very high element specificity.

5.2 Hysteresis

In order to demonstrate the feasability of XMOKE for recording element-specific hysteresis loops from lanthanide systems a Gd/Y/Tb multilayer film was grown *in situ* on a W(110) substrate (thickness of 5 nm/ 2 nm/ 10 nm). The hysteresis loops are shown in Fig. 5.4. The upper loop was recorded at $h\nu$ = 147 eV (at the giant-resonance peak of Gd, see Fig. 5.2) and the lower spectrum was taken at $h\nu$ = 176 eV (at the trailing edge of the giant-resonance peak of Tb), both at a sample temperature of 195 K. While the 147-eV loop reveals mostly the Gd magnetization as a function of the external field the 176-eV loop is predominantly caused by the Tb magnetization. However, it contains also a sizable signal from the Gd magnetization. Clearly the two lanthanide films are characterized by widely different coercive fields $H_C^{Gd} = (96 \pm 3)$ Oe and $H_C^{Tb} = (480 \pm 20)$ Oe. In the central panel (b) 'pure' Gd and Tb hysteresis loops are shown; they were obtained from the experimental spectra in (a) by creating adequate linear combinations (this is only an approximate procedure.) In panel (c) XMOKE loops of the same multilayer are shown, recorded at a sample temperature of 172 K in the $M_{4,5}$-threshold regions: at $h\nu$ = 1184 eV (upper, Gd M_5 peak) and at $h\nu$ = 1239 eV (lower, Tb M_5 peak). Here a complete elemental separation is obviously achieved. Based on absorption data from magnetized Gd and Tb films [49,101,161,164] the effective XMOKE information depth was estimated,

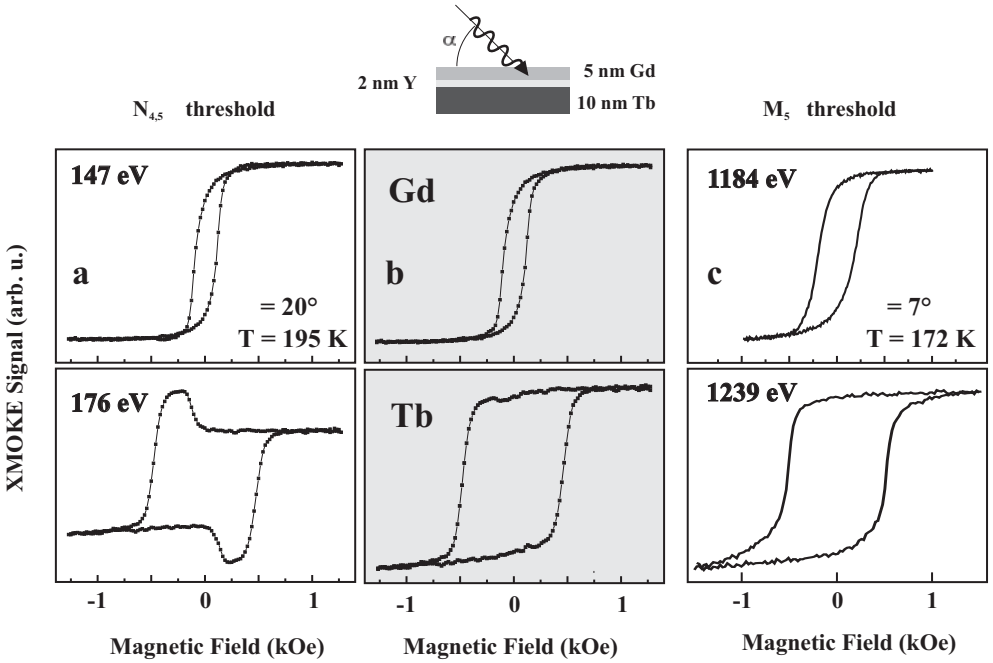

Figure 5.4. Hysteresis loops recorded from a Gd/Y/Tb trilayer, using the specularly reflected cp-polarized x-ray intensity, (a) in the $N_{4,5}$-edge energy range and (c) at the M_5 edges of Gd and Tb. (b) shows linear combinations of the raw $N_{4,5}$ loops from (a).

including the effect of grazing light incidence, for Gd to be about 2 nm (14 nm) at a photon energy of 147 eV (176 eV), and 14 nm (10 nm) for Tb at the same energies. At the Gd M_5 peak (7° light incidence) the estimate was 1.2 nm (∼100 nm) for Gd (Tb), compared to ∼16 nm (∼1.2 nm) at the Tb M_5 peak [164]. The slightly different shapes of the hysteresis curves in Figs. 5.4(b) and 5.4(c) mainly reflect the higher coercivities at lower temperature.

5.2.1 Influence of domain-wall movements

In accordance with the strong in-plane anisotropy of Tb, the magnetic domain walls, which separate two directions of magnetization, must lie within the basal plane of the Tb hcp lattice (see section 2.4.3). Experimental studies revealed a regularly sliced pattern along the *c*-axis with only small differences between *a*- and *b*-directions [82]. The patterns in the basal planes consist of markings parallel to the three directions at angles of 120° with respect to each other [83]. Theoretical calculations based on the minimization of magnetostrictive and exchange energy lead to the prediction of 180° walls along the *c*-direction with a wall thicknesses of 20 ML [1] [81].

Below 244 K the magnetic moments in Gd bulk crystals undergo a reorientation out of the basal plane towards the *c*-axis (cf section 4.3). As known from the thickness dependence of the spin-reorientation temperature (cf. section 4.3), in thin Gd films ($d \leq 30$ nm) the

[1] This matches the helical period of the Tb AF phase.

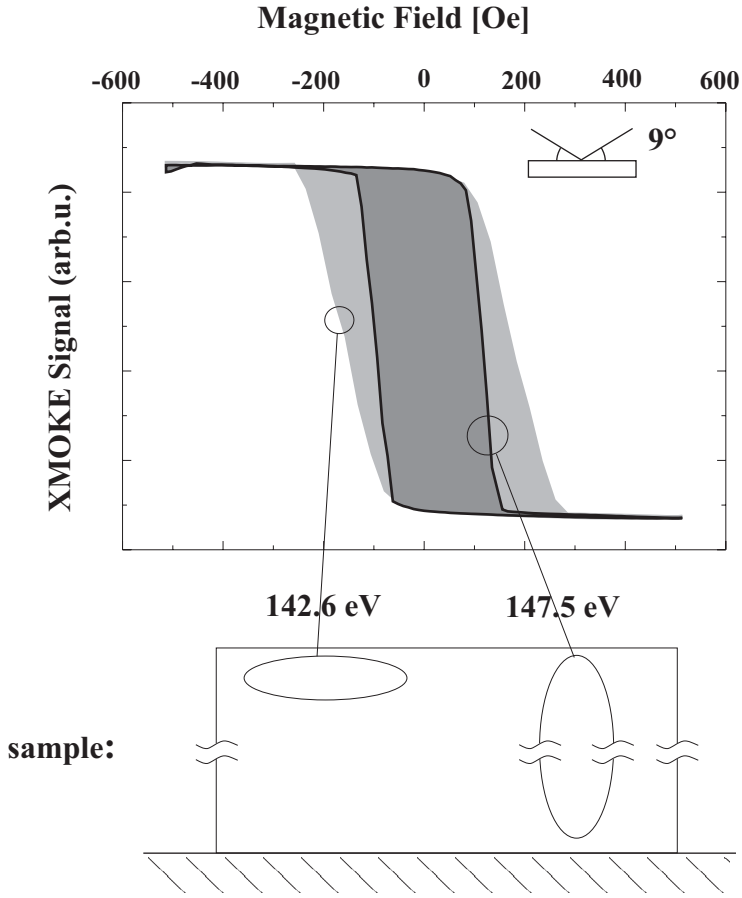

Figure 5.5. XMOKE signal from an 8-nm thick Gd film on W(110) recorded at 147.5 eV and 142.6 eV photon energies at grazing incidence (9°). At small angles the perpendicular component of the light beam is small, and the dichroic difference in the penetration depth is less important.

spins are restricted to the basal plane (as in Tb), and we may expect that the domain walls behave similarly to those observed in Tb.

How does the domain wall movement affect the connection of magnetization and XMOKE signal during the reversal of magnetization? If the XMOKE signal contains equal contributions from all atomic layers, the actual magnetization reversal process of the whole system will be imaged by a change in the intensity of the reflected light regardless in what direction the domain walls propagate (the loss/gain in light intensity goes with the fraction of reversed magnetization). This is not the case when the absorption is strong, and the light is significantly damped; then the reflected light images mainly the behavior of the topmost layers. Supposed that the domain walls propagate perpendicular to the film plane then – during the reversal of the magnetization – one would always see the same image no matter how deep one looks into the crystal. In case of strong absorption the signal contains mainly light reflected at the topmost layer(s). In case the domain walls propagate along the c-axis, i.e. the magnetization reverses quasi layer-by-layer, the top layers(s) either reverse first or last (depending on the propagation of the domain walls). If the coercive field is smeared

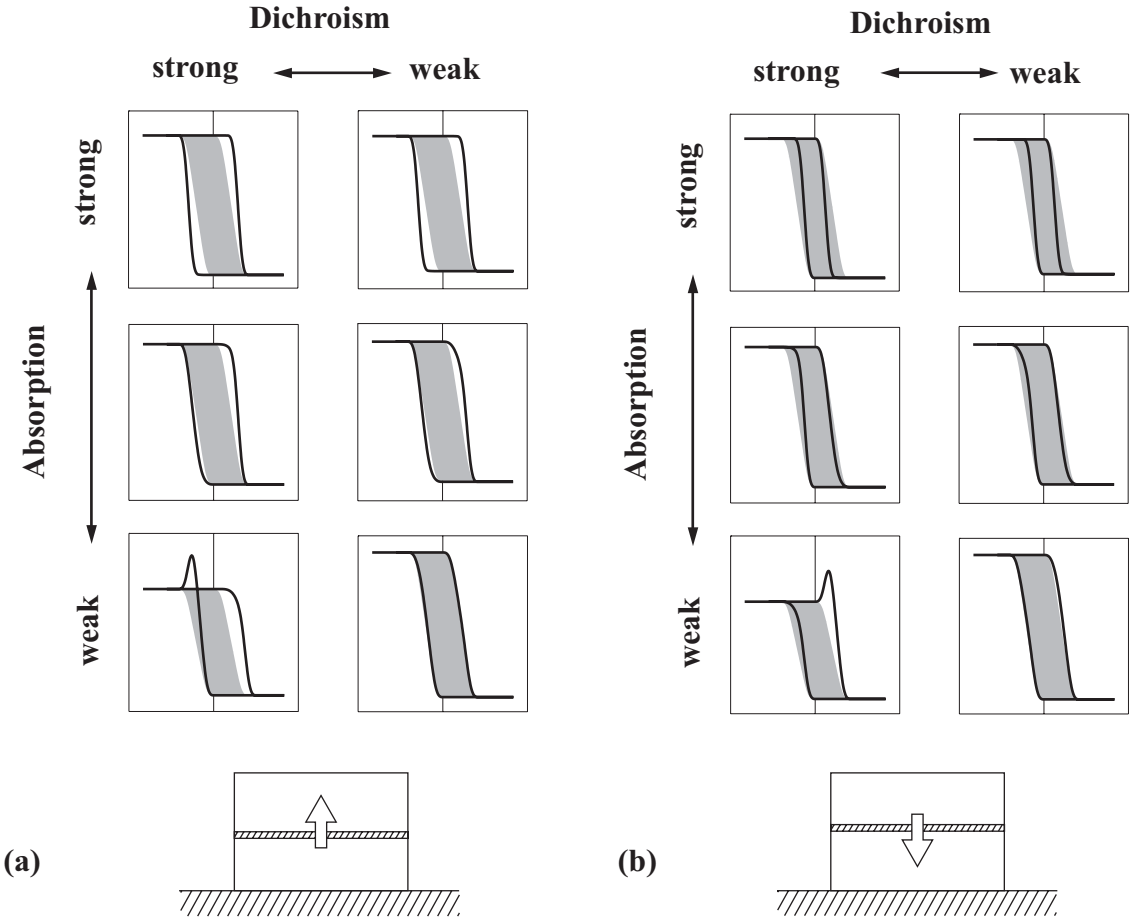

Figure 5.6. A simple model describing the expected XMOKE-signal (thick line) as it should be obtained from a given magnetization reversal (shaded area) under the assumption that the domain wall propagates along the c axis (a) from the substrate towards the film surface or (b) from the surface down to the substrate.

out (e.g. due to a strain gradient along the *c*-axis) the signal images mainly the beginning (or the end) of the reversal process, hereby reflecting a larger (or smaller) coercive field as compared to the real one.

When the magnetic contrast in the signal is large, the penetration depth strongly depends on magnetization, and therefore contributions of opposite magnetizations are not equally weighted; this causes a deviation between the dichroic signal and the magnetization of the sample.

In order to verify this hypothesis it is reasonable to argue with the help of a model which is able to describe the reversal of the magnetization in the observed system. In accordance with the experimentally observed domain structure [82, 83], a model is proposed where the sample is virtually divided into slabs parallel to the basal plane of the Tb hcp structure. The polarization of light (right or left circularly polarized) is assumed to be parallel or antiparallel to the magnetization direction, giving a dichroic reflection and transmission at

each slab. The effect of the substrate-induced strain is taken into account by assuming a coercive field gradient along the c-axis. This causes each slab to reverse its magnetization at a different magnetic field H_i, with the condition $H_1 < H_2 < H_3 < ..$ for successive slabs, resulting in a step-by-step reversal of the basal-plane magnetization with increasing field. (The result is that a Bloch wall lies in the basal plane and moves along the c-axis as suggested earlier [165].) Results of the proposed model for upward and downward moving walls, at strong and weak absorption combined with big and small dichroic effects, as can be found by an appropriate choice of the photon energy, are presented in Fig. 5.6. If the process of magnetization reversal starts in the downmost slab, the XMOKE signal should behave as shown in Fig. 5.6(a). For the opposite case (reversing first the topmost slab) the expected XMOKE signal is shown in Fig. 5.6(b). The main difference between the two cases is that (a) the image hysteresis of a domain wall moving *upward* seems to have a bigger coercive field as compared to the real H_C, while (b) a *downward* moving domain wall produces a smaller H_C.

As an example a hysteresis loop of Gd/W(110) recorded at photon energies of 142.6 eV (pre-edge) and 147.5 eV (giant absorption) is shown in Fig. 5.5. At 147.5 eV, the absorption is huge and all the light is mainly reflected from the topmost surface layers, whereas at 142.6 eV the absorption is comparable to the visible-light region, and the obtained signal consists of almost equal contributions of all layers. In the first case, we see mostly the magnetization of the topmost layers, whereas the second case reflects the magnetization of the whole system. The overall magnetization reveals a lower coercive field as compared to the magnetization of the topmost layers. A comparison with the model shows that Gd the magnetization of the Gd film obviously reverses by domain walls propagating from the substrate to the surface.

5.2.2 Photon energy dependence

The model in the previous section suggests that during magnetization reversal the XMOKE signal is approximately proportional to the magnetization if either the signal originates from the whole sample or if the observed part of the sample shows the same behavior as the entire sample. The first statement refers to the optical properties of the sample, the second to the magnetization-reversal process. The whole sample (model: all layers) is observed if the penetration depth is large, i.e. the absorption is weak. Furthermore, the absorption should ideally be the same for both magnetization directions up and down spin in order to obtain an equally weighted signal from both; yet this requirement would inevitably lead to vanishing dichroism.

Fig. 5.7 shows hysteresis loops of a 10-nm Tb/W(110) film measured at different photon energies, together with the associated absorption and dichroism curves measured in reflection. At 149.4 eV the absorption is weak, and at the same time the dichroism is small (Fig. 5.7(b)). The dichroic signal thus comes from the entire film and structural inhomogeneities leading to a discrepancy between local and general view do not disturb. This hysteresis, showing no asymmetries, is considered to be the 'true hysteresis' and will be taken in the following as the reference to compare with.

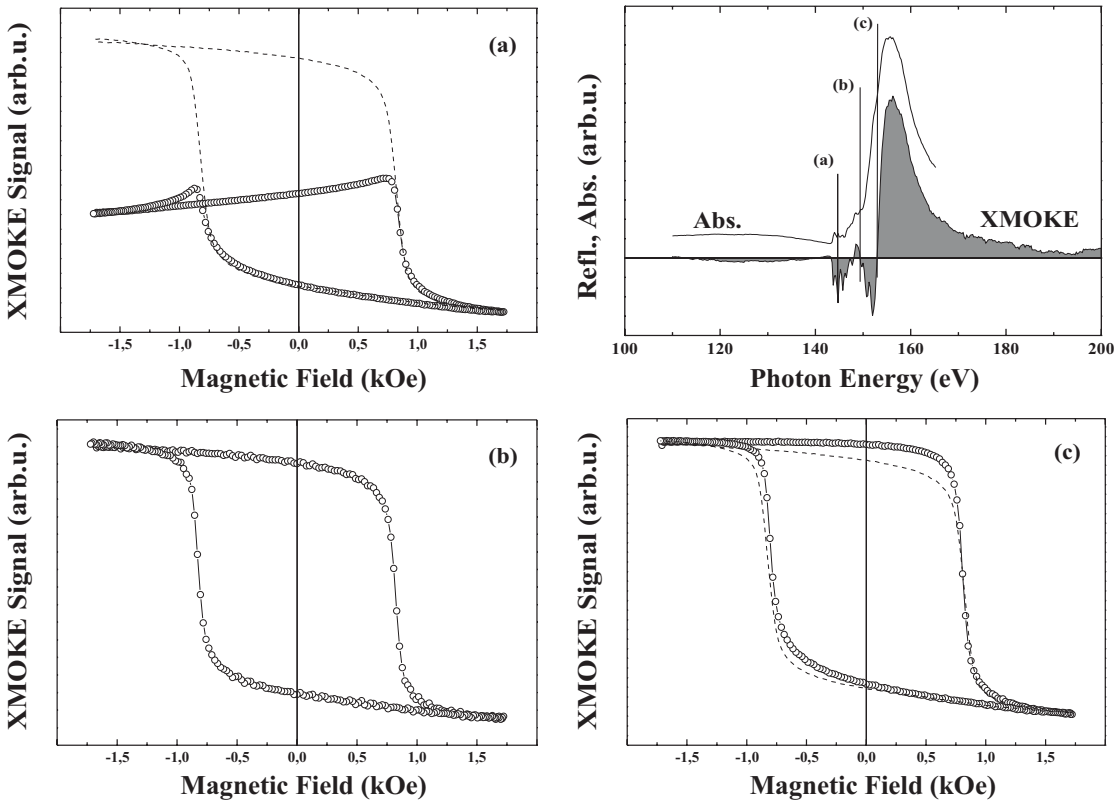

Figure 5.7. XMOKE hysteresis of 10 nm Tb/W(110) at different photon energies: (a) 144.7 eV, (b) 149.4 eV, and (c) 152.9 eV. The angle between incident light and surface plane was 30°. (a) and (c) are shown in comparison with (b) (dashed line). The dichroic signal in reflection (XMOKE) together with the integral absorption (Abs.) is depicted in the upper right panel.

In Fig. 5.7(a) the absorption is weak, but the dichroism is substantial. The lower part of the hysteresis is virtually identical with 5.7(b) until approximately half of the film magnetization is reversed and the optical conditions change drastically. The substrate becomes visible (invisible) as the magnetization reverses, leading to strong changes in the interference between light reflected at the film and at the substrate. This leads to the observed anomaly in the hysteresis. Note that the occurrence of such an interference effect is *independent* of the direction of the domain wall movement.

Vanishing dichroism together with strong absorption leads to a hysteresis as shown in Fig. 5.7(c). Here the probing x-ray beam decays strongly with increasing thickness. The image obtained is close to (b) but shows asymmetric features as well as a slightly reduced coercive field. This is due to the fact that (b) shows the magnetization of the whole sample, while (c) only reflects that of the top layers. The measured reduced coercivity in (c) shows that the magnetization reversal in Tb/W(110) - contrary to Gd/W(110) - starts obviously with the topmost layer. The asymmetry upon reversal originates from the magnetization-dependent penetration depth, i.e. for one orientation of the magnetization one looks deeper into the film than for the other.

5.3 The optical constants

Several studies have shown that in order to analyze soft x-ray MO signals from thin films and multilayer systems with thicknesses comparable to the probing wavelength and to extract a layer-resolved sample magnetization profile, a comparison with model calculations of the reflected specular intensity (based on the Fresnel equations) is needed [20, 28, 33]. Several experimental determinations of soft x-ray magneto-optical constants have been reported for $L_{2,3}$ threshold regions of ferromagnetic transition metals but none so far for the lanthanide elements [23, 24, 31]. In this section calculations of the optical constants of thin Gd/W(110) films at the $N_{4,5}$ absorption thresholds are presented.

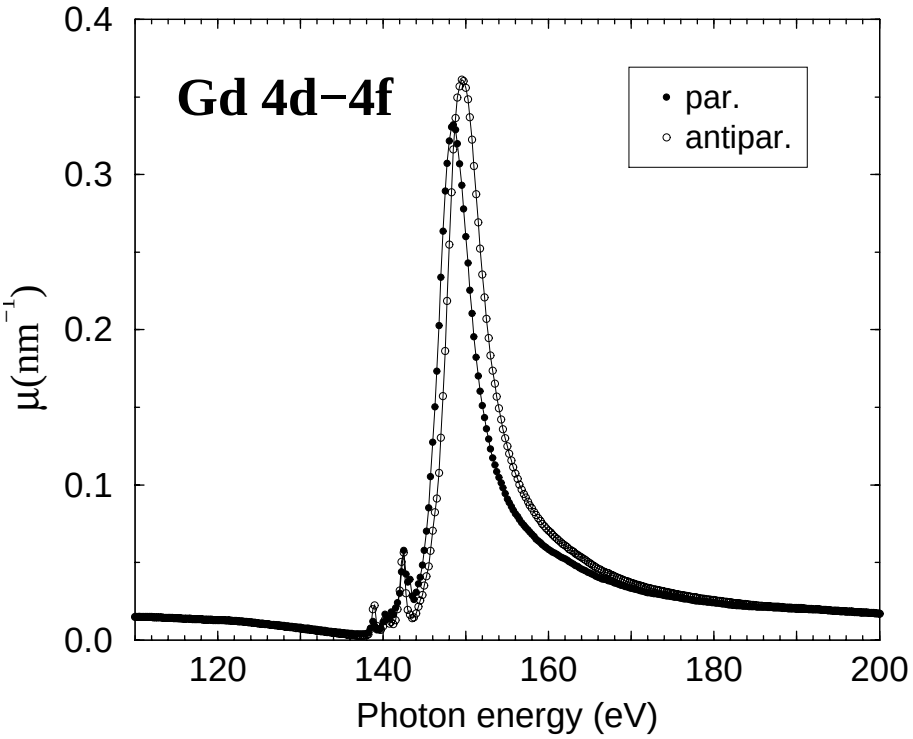

Figure 5.8. Gd $N_{4,5}$ absorption spectra from remanently magnetized Gd films at $T = 30\ K$. CP light was incident at 30° with respect to the film plane, i.e. mainly parallel (filled symbols) and antiparallel (open symbols) to the in-plane sample magnetization.

Figure 5.8 displays experimental absorption spectra in the region of the Gd $N_{4,5}$ threshold. The spectra were corrected for saturation [166, 167] assuming a value of 0.3 for the ratio of electron escape depth to minimal X-ray absorption length. The photon energy range of the present spectra is significantly wider than in previous studies [101, 168] including the wide asymmetric flanks of the 4d → 4f giant resonance (Beutler-Fano profile). This allows one to calibrate the absorption spectra by matching both ends to the tabulated absorption coefficient [34] at photon energies where the influence of the giant resonance is expected to be negligible. To this end we fixed the absorption coefficients $\mu_{\pm}$ at the

low-energy (110 eV) and the high-energy sides (200 eV) of the measured spectra to the values given by the tables of Henke *et al.* [34], 15.0 and 17.1 $\times 10^{-3}$ nm^{-1} at 110 and 200 eV, respectively. This then defines the given scale of the ordinate in Fig. 5.8. The absorption coefficient is obtained with an error bar of $\pm 15\%$ in the peak, estimated from the experimental precision of $\pm 1\%$ at both ends of the photon energy range which were adjusted to the tabulated data. Note that the spectra in Fig. 5.8 show the same qualitative energy dependence as given earlier [101], yet the previous spectra were scaled to the same maximum value for both magnetization directions without any correction for saturation effects.

The comprehensive X-ray data tables of Henke *et al.* [34] contain the lanthanide $N_{4,5}$ absorption spectra by Zimkina *et al.* [169] who measured *relative* linear X-ray absorption lengths of non-magnetized lanthanide samples. In order to extract an absolute absorption length from these data Henke *et al.* [34] followed Richter *et al.* [170] who calibrated their gas-phase photoexcitation data by adjusting them to calculated cross sections. They determined a maximum absorption coefficient at the nonmagnetic Gd $N_{4,5}$ peak of $\mu \approx 0.1$ nm^{-1}, corresponding to a linear X-ray absorption length $l_{abs} = 1/\mu \approx 10\ nm$ [34]. By contrast the calibrated experimental spectra from magnetized Gd in Fig. 5.8 reveal maximum values for the absorption coefficient of 0.33 nm^{-1} and 0.36 nm^{-1} for nearly parallel and antiparallel orientation of sample magnetization and photon spin, respectively. The corresponding linear absorption lengths are 3.0 nm and 2.8 nm, with the quoted error of $\pm 15\%$; they are about three times shorter than expected [34]. These soft X-ray absorption lengths are remarkably short, even compared with visible-light absorption lengths in metals of typically some 20 nm.

The difference spectrum $\Delta\mu(\omega) \equiv (\mu_+(\omega) - \mu_-(\omega))/\cos(30°)$ obtained from the experimental absorption spectra $\mu_\pm(\omega)$ is displayed in Fig. 5.9(a). The factor $1/\cos(30°)$ accounts for the finite experimental angle between the directions of light propagation and magnetization. Apart from minor contributions from the weaker pre-edge transitions around 140 eV (inset of Fig. 5.9(b)) the $\Delta\mu(\omega)$ spectrum exhibits an S-shape behavior, with a zero crossing near 149 eV.

It originates from the very intense $4d^{10}\ 4f^7[^8S] \rightarrow 4d^9\ 4f^8[^8P]$ transitions (dipole allowed in LS coupling). For *parallel* orientation of photon spin and sample magnetization ($\Delta M = +1$ transitions) the intermediate $^8P_{5/2}$ state at around 148 eV is preferentially populated. For *antiparallel* orientation ($\Delta M = -1$ transitions) by contrast the only allowed excitation is into the $^8P_{9/2}$ state at around 150 eV [101]. The large difference in absorption coefficient for opposite magnetization directions (Fig. 5.9(a)) corresponds to a difference in the absorptive part $\Delta\beta \equiv \beta_+ - \beta_- = \Delta\mu\,\lambda/(4\pi)$ of the refractive index $n_\pm = 1 - \delta_\pm + i\beta_\pm$. As shown in Fig. 5.9(b) $\Delta\beta$ changes from $+0.082$ to -0.085 within 3.5 eV.

From the present data the associated difference in the real part, $\Delta\delta \equiv \delta_+ - \delta_-$, for CP light propagating (exactly) parallel or antiparallel to the Gd magnetization was derived using the Kramers-Kronig (KK) transformation for magnetic systems [171] (the result is shown in Fig. 5.9 by open symbols). The accuracy of this integral transformation depends mainly on the spectral range available for integration. Within the extended photon energy range from 110 to 200 eV the absorption spectra recorded for opposite magnetization

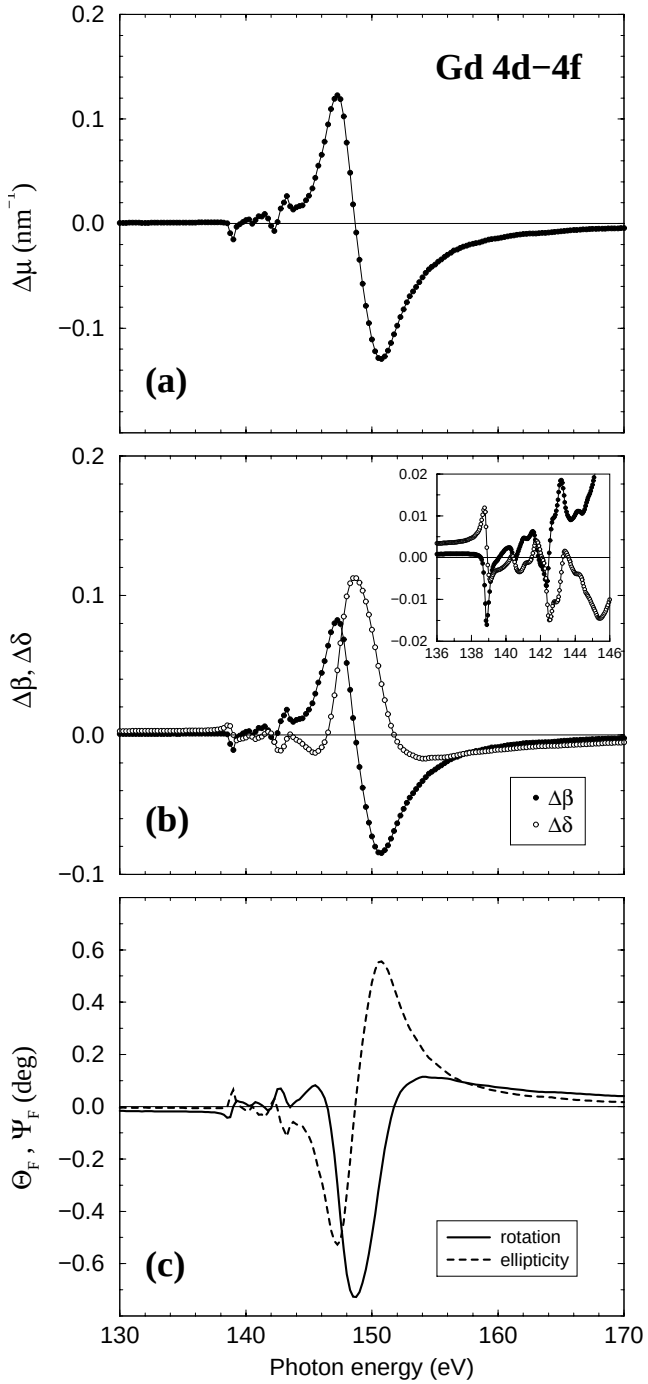

Figure 5.9. (a) Difference spectrum $\Delta\mu(\omega) \equiv (\mu_+(\omega) - \mu_-(\omega))/\cos(30°)$ of the absorption spectra for opposite magnetizations given in Fig. 5.8. (b) Difference $\Delta\beta$ of the imaginary parts (filled symbols) and the associated difference $\Delta\delta$ of the real parts (open symbols) obtained through Kramers-Kronig transformation. Inset: pre-edge region, measured ($\Delta\beta$, filled symbols) and calculated ($\Delta\delta$, open symbols) with higher point density. (c) Faraday rotation and ellipticity spectra calculated for linearly polarized light transmitted normally through a 0.3-nm thick Gd metal film which is magnetized perpendicular to the film plane.

directions appear to become asymptotically equal at both ends of the studied photon-energy range (see Fig. 5.8). Hence the difference $\Delta\beta$ vanishes at the two boundaries of the KK transformation, the result is not affected by the specific choice of the studied photon energy range. The phase difference $\Delta\delta$ peaks right at the zero crossing of the absorptive part where it amounts to $\Delta\delta \approx 0.11$ (see Fig. 5.9(b)).

$4d-4f$ threshold region		
$h\nu$	Gd	Tb
110 eV	70 nm	60 nm
anti-resonance	200 nm	140 nm
pre-peak	20 nm	33 nm
peak (parallel)	3.3 nm	5.6 nm
peak (anti-parallel)	3.0 nm	7.7 nm
200 eV	60 nm	50 nm

$3d-4f$ threshold region		
$h\nu$	Gd	Tb
$<M_5$	700 nm	770 nm
M_5 peak (parallel)	8.4 nm	7.0 nm
M_5 peak (antiparallel)	15 nm	15 nm
between M_5 and M_4	300 nm	350 nm
M_4 peak (parallel)	30 nm	30 nm
$> M_4$	130 nm	160 nm

Table 5.1. Calculated absorption lenghts l_{abs}.

For future applications the complex Faraday rotation (FR) of Gd metal was calculated using the experimental difference in the absorptive part $\Delta\beta$ together with the calculated phase difference $\Delta\delta$ assuming perfect alignement of the $4f$ magnetic moments as existing, e.g. in the ferromagnetic phase at low temperatures ($T/T_C \ll 1$). Real and imaginary parts of the FR Θ_F and Ψ_F respectively are given by the expressions [172]

$$\tan(2\Theta_F) = 2\,Re\,[a]\,/(1-|a|^2)\,, \tag{5.2}$$

$$\sin(2\Psi_F) = 2\,Im\,[a]\,/(1+|a|^2)\,, \tag{5.3}$$

where $a = \tan(\Delta n \omega d/c)$, d is the film thickness, and $\Delta n = (n_+ - n_-)/2$. The $\Theta_F(\omega)$ and $\Psi_F(\omega)$ spectra of Gd metal at the $N_{4,5}$ threshold are presented in Fig. 5.9(c) for linearly polarized (LP) light transmitted in normal direction through a 0.3 nm (1 monolayer) thick Gd metal film magnetized perpendicular to the film plane either *parallel* or *antiparallel* to the light propagation direction. The spectra predict a specific Faraday rotation of $\Theta_F = (0.73 \pm 0.11)^\circ$ per 0.3 nm ($2.4 \pm 0.4^\circ/nm$) near 149 eV right at the zero crossing of the absorption difference for CP light in Fig. 5.9(a). At this photon energy Θ_F is accompanied by a vanishing Faraday ellipticity Ψ_F (cf. Fig. 5.9(c)).

The reported specific FR is nine times larger than the specific rotation maximum found previously at the Fe L_3 threshold [25] and some 70 times (50 times) larger than in the visible (infrared) region of Fe metal. The huge FR at Gd $N_{4,5}$ is due to the very large electric dipole (E1) transition probability of $4d^{10}\ 4f^n \rightarrow 4d^9\ 4f^{n+1}$ transitions ($n = 7$ for Gd). Hence the strong absorption at the Gd $N_{4,5}$ giant-resonance peak (cf. Fig. 5.8) leads to a very short penetration length of the order of only 3 nm. In order to obtain e.g. a FR of $\pm 45^\circ$ for opposite film magnetizations one would need an 18.5 nm thick Gd film leading to an inevitable intensity reduction by a factor of $4.5 \cdot 10^2$. Despite this substantial loss in intensity which results in a transmitted flux of about 10^{11} photons/(s $\cdot$ 100 mA $\cdot$ 0.1% bandwidth) at

a typical third-generation undulator beamline Gd films might well be useful in differential (lock-in technique) experiments where *fast switching* of the X-ray polarization plane (ns time scale) is required. The photon energy range of this method could be extended to about 180 eV [34] by using heavier lanthanide elements.

5.4 Calculated reflectivities and interference effects

From soft x-ray reflectivity analysis at transition metal $L_{2,3}$ edges it is known that the XMOKE signal is subject to interference effects [20]. They destroy the simple linear relation between XMOKE signal and sample magnetization, and can severely complicate the interpretation [29]. Using the optical constants β and δ (see section 5.3) one can calculate the intensity of the light reflected at the sample for a given energy and angle of incidence. In this section the magnetization dependent optical constants of Gd and Tb metal at the $M_{4,5}$ and $N_{4,5}$ absorption thresholds are presented, from which reflectivity spectra are calculated and compared with experimental measurements.

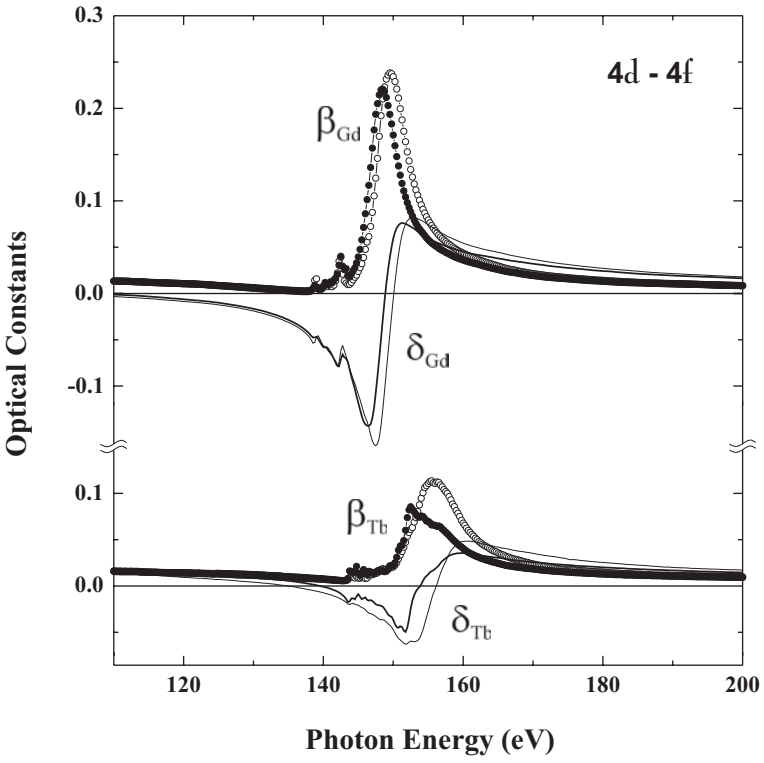

Figure 5.10. The optical constants β and δ of Gd and Tb at the $N_{4,5}$ absorption threshold. The parallel β^+ (•) and antiparallel β^- (∘) indicate the relative orientation of magnetization and direction of light propagation. The related dispersions are denoted δ^+ (thick line) and δ^- (thin line). Note that the absorption peaks of Gd and Tb are separated by ~ 10 eV which is in the same order of magnitude as the peak width [175].

The absorptive (β) and dispersive part (δ) of the refractive index $n = 1 - \delta + i\beta$ are related through Kramers-Kronig transformation (KKT) [43] which permits to simulate $M_{4,5}$ XMOKE spectra just on the basis of an absorption measurement. Usually the absorption β is determined in transmission experiment (Faraday) [169,170,173]. However, the reflectivity rapidly drops in intensity as one goes from grazing to normal incidence, and its effect to the measured electron yield becomes negligible ($yield = (1 - R) \times \sigma_{auger}$). At finite angles

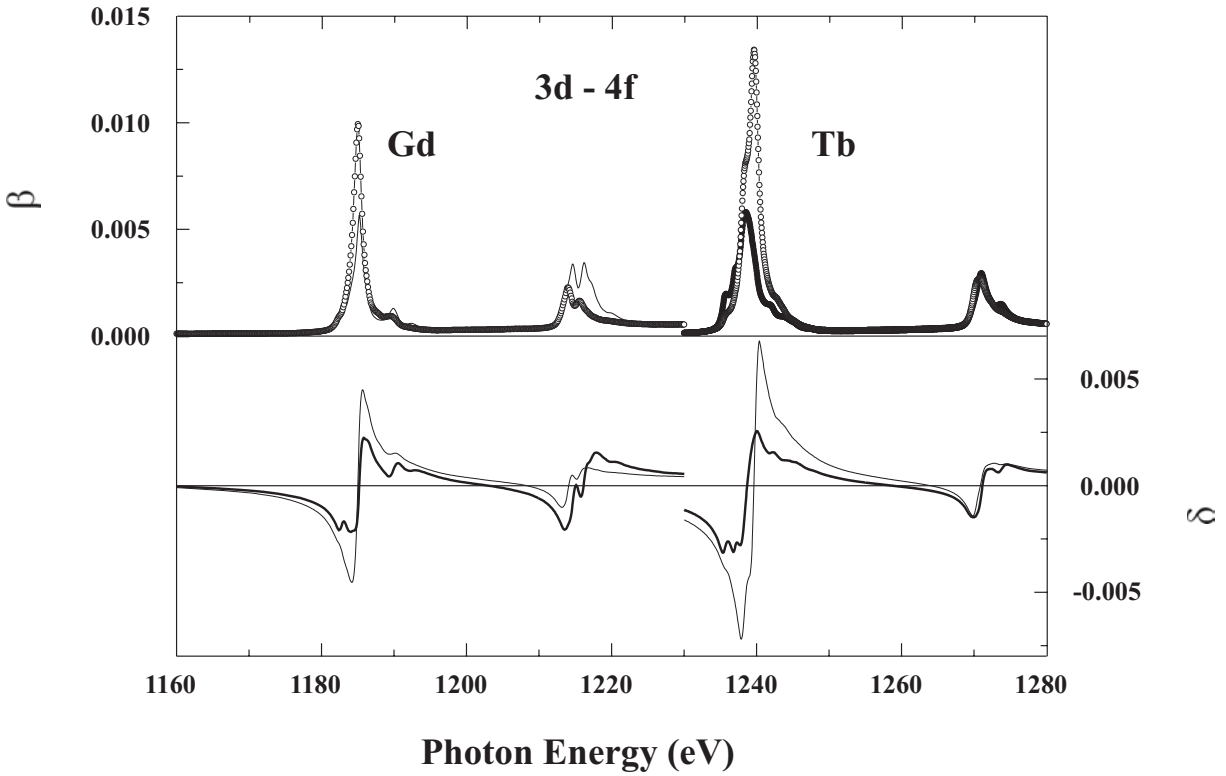

Figure 5.11. The optical constants β and δ of Gd and Tb at the $M_{4,5}$ absorption threshold. The parallel β^+ (•) and antiparallel β^- (∘) indicate the relative orientation of magnetization and light propagation direction. The related dispersions are denoted δ^+ (thick line) and δ^- (thin line). Note that the absorption peaks of Gd and Tb are widely separated by ~ 30 eV.

($\geq 20°$) the reflectivity is already some orders of magnitude smaller, and one can use in good approximation the electron yield obtained in a reflection experiment [102].

Fig. 5.10 shows the optical β of Gd and Tb obtained from experimental $N_{4,5}$ absorption spectra with CP x-rays from magnetized Gd/W(110) films for opposite magnetization directions, either nearly parallel (β^-) or antiparallel (β^+) to the light propagation direction. The energy dependence of the associated dispersive spectra ($\delta^\pm$) calculated via KKT is shown in the same Figure. The related dispersion (δ) is obtained by the Kramers-Kronig relation [43, 75]. The shape of the absorption is characterized by the Beutler-Fano profile originating from the interference of two excitation paths: (1) direct excitation $4f \rightarrow vacuum$ and (2) virtual excitation $4d \rightleftarrows 4f$ plus Auger-decay into the continuum [49]. Due to the relatively weak spin-orbit coupling constant in the $4f$-shell ($\xi_{SO} \approx 2$eV for Gd), the multiplet lines of ($4d^9 4f^8$) are spread over about 10 eV by the strong Coulomb correlation between d and f electrons of the same principal quantum number $n = 4$ giving one broad absorption peak (Fig. 5.10). The spectra of both elements on the same energy scale shows that the absorption maxima of β_{Gd} and β_{Tb} are separated by a few eV which impedes a good energy separation.

At the $M_{4,5}$ absorption threshold the direct excitation channel $4f \rightarrow vacuum$ has

become unimportant and the line shape is Lorentzian [49]. The multiplet is characterized by the spin-orbit coupling in the $3d$-band with a coupling constant $\xi_{SO} \approx 30$ eV revealing a well separated two-line structure (Fig. 5.11). The optical behavior at the $M_{4,5}$ absorption threshold is nicely described by the oscillator model. Below the resonance the dispersion shows an "air-to-water" behavior ($n > 1$) and changes to a "water-to-air" behavior ($n < 1$) above the resonance. Right at resonance the absorption shows a sharp peak, decaying fast in going off-resonance. The dispersion decreases much more softly, and off-resonance the usual approximation $n \approx 1 - \delta$ is valid. Compared to the $N_{4,5}$ threshold region the magnitude of the $M_{4,5}$ absorption peak is smaller by a factor of 10 (antiparallel) to 20 (parallel) for both elements. The energy difference of the absorption maxima of Gd and Tb is ∼50 eV which will be useful to completely separate elemental contributions to the magnetization-reversal process in heteromagnetic systems, e.g. in a layered Gd/Tb compound.

The reflected light intensity at the interface between two media with different indices of refraction is described by the Fresnel equations [43, 44]. In order to describe the reflectivity of a layered systems one refers to a simple continuum approach where each layer is considered to be a slab with homogeneous optical properties; the light is reflected at the interface between two slabs of different indices of refraction. From the superposition of the complex amplitudes from each slab, multiplied by its complex conjugate, one obtains the total reflected light intensity. A single thin film deposited on a substrate is thus thought as being a system consisting of two slabs, where the thickness of the second slab (substrate) is semi-infinite. The scheme of such a system is depicted in Fig. 5.12.

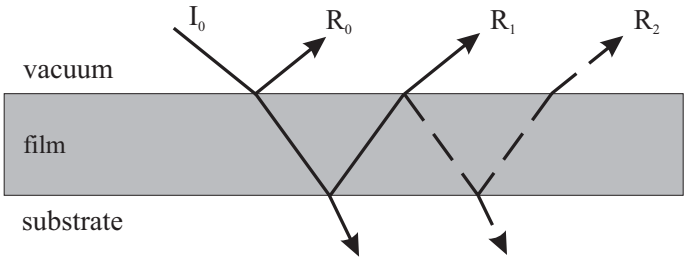

Figure 5.12. Scheme of the reflectivity model for a flat film deposited on a semi-infinite substrate. In the continuum approach each medium (vacuum - film - substrate) is homogeneous and has a specific index of refraction. The reflection occurrs at the interface between two media.

The knowledge of the index of refraction enables one to calculate the expected reflectivity from a sample for a given angle and photon energy. One has to be aware that the reflected light from the substrate is again partially reflected at the film/vacuum interface leading to multiple-reflection terms in the total reflected signal. The total reflection can be written as

$$R_{tot} = R_{film}^{vac} + T_{film}^{vac} \cdot A \cdot R_{sub}^{film} \cdot A \cdot T_{vac}^{film} + mult.refl. \tag{5.4}$$

with R being the reflectivity, T the transmission, and A the absorption in the film. If the film has a weak absorption and if the index of refraction of the substrate is comparable

to that of the vacuum, multiple reflections become important (Fabry-Perrot). This could be the case in the pre-peak region of the $4d-4f$ excitation where the optics between film and substrate are comparable to the "water-to-air" situation. In the following the multiple reflection term is omitted since it only reveals a quantitative amelioration of the result (line sharpening).

In Fig. 5.13 experimental reflected light intensity at the $N_{4,5}$ and $M_{4,5}$ absorption thresholds of a thin Gd film (nm-range) on W(110) are compared with calculated reflectivities. At the $M_{4,5}$ absorption thresholds one observes a fairly good agreement between theory and experiment. The peaks in the experimental spectrum are obviously broader than the calculated linewidth, most likely due to the limited accuracy of the angle adjustment in the experiment as well as incoherent scattering contributions to the reflected light intensity. But the most important features like peak position, pre-shoulder, and relative peak heights agree well in the experimental and calculated spectra.

Similarly good results cannot be achieved at the $N_{4,5}$ thresholds. Using experimentally determined β's and KKT, line parameters for the Gd $M_{4,5}$ and $N_{4,5}$ excitation thresholds yield a roughly constant lifetime at the $M_{4,5}$ threshold ($\tau = 1.6 \cdot 10^{-16}$ s) but a factor of ~ 20 difference between pre-peaks ($\tau_{pp} = 2 \cdot 10^{-15}$s) and the giant-resonant ($\tau_g = 9 \cdot 10^{-17}$s) at the $N_{4,5}$ edge. This vast difference in core hole lifetime at the $N_{4,5}$ thresholds is mainly caused by the super Coster-Kronig Auger decay that does not contribute to the β which is relevant for the reflectivity. Therefore the measured β_{exp} and the β used in optics are likely not to change in the same way when going from the pre-region to the giant-resonant region. (For the linewidth and the resulting lifetimes cf. Ref. [49].)

The relative importance of the substrate contribution to the total reflectivity is shown in Fig. 5.14 for a 8 nm thick Gd film on a W(110) substrate at the $M_{4,5}$ absorption threshold. The resonances of the substrate are far away, so that $n \approx 1 - \delta$ is a reasonable approximation. One can apply with the oscillator model assuming a single oscillator at the Gd M_5 (or M_4) resonance. At the film/substrate interface light propagates from a less dense into a more dense medium which in the regime of normal refraction (just before the resonance) leads to an "air-to-water" like situation. After the resonance the situation is reversed ("water-to-air"), and the substrate becomes quasi invisible. This can nicely be seen when comparing total reflectivity and contributions from the substrate: above and below resonance the light intensity is approximately the same but the contribution from the substrate just above resonance almost disappears (see Fig. 5.14).

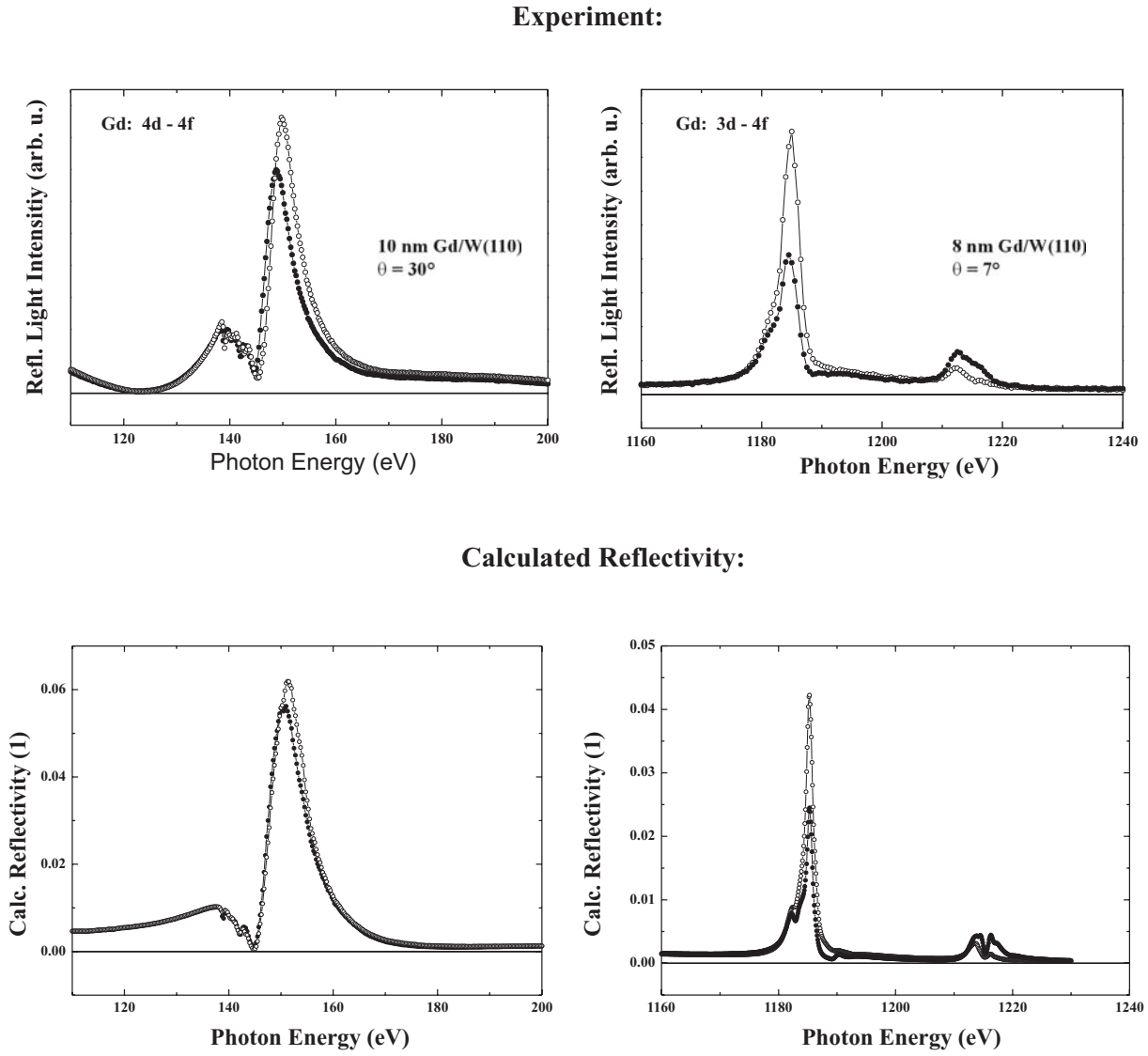

Figure 5.13. Experimental reflectivities at the Gd N_5 and $M_{4,5}$ absorption threshold are shown in the upper-left and upper-right panel, respectively. The sample was magnetized in remanence along the easy axis of magnetization. The magnetic contrast was obtained by reversing the magnetization where parallel (•) and antiparallel (◦) indicate the relative orientation of magnetization and the Pointing vector of the light. Corresponding calculated reflectivities (Fresnel equations) from experimentally determined β's (obtained from absorption measurements) and their related δ's (derived by the Kramers-Kronig relation) at the Gd N_5 and $M_{4,5}$ absorption thresholds are depicted in the lower-left and lower-right panel, respectively.

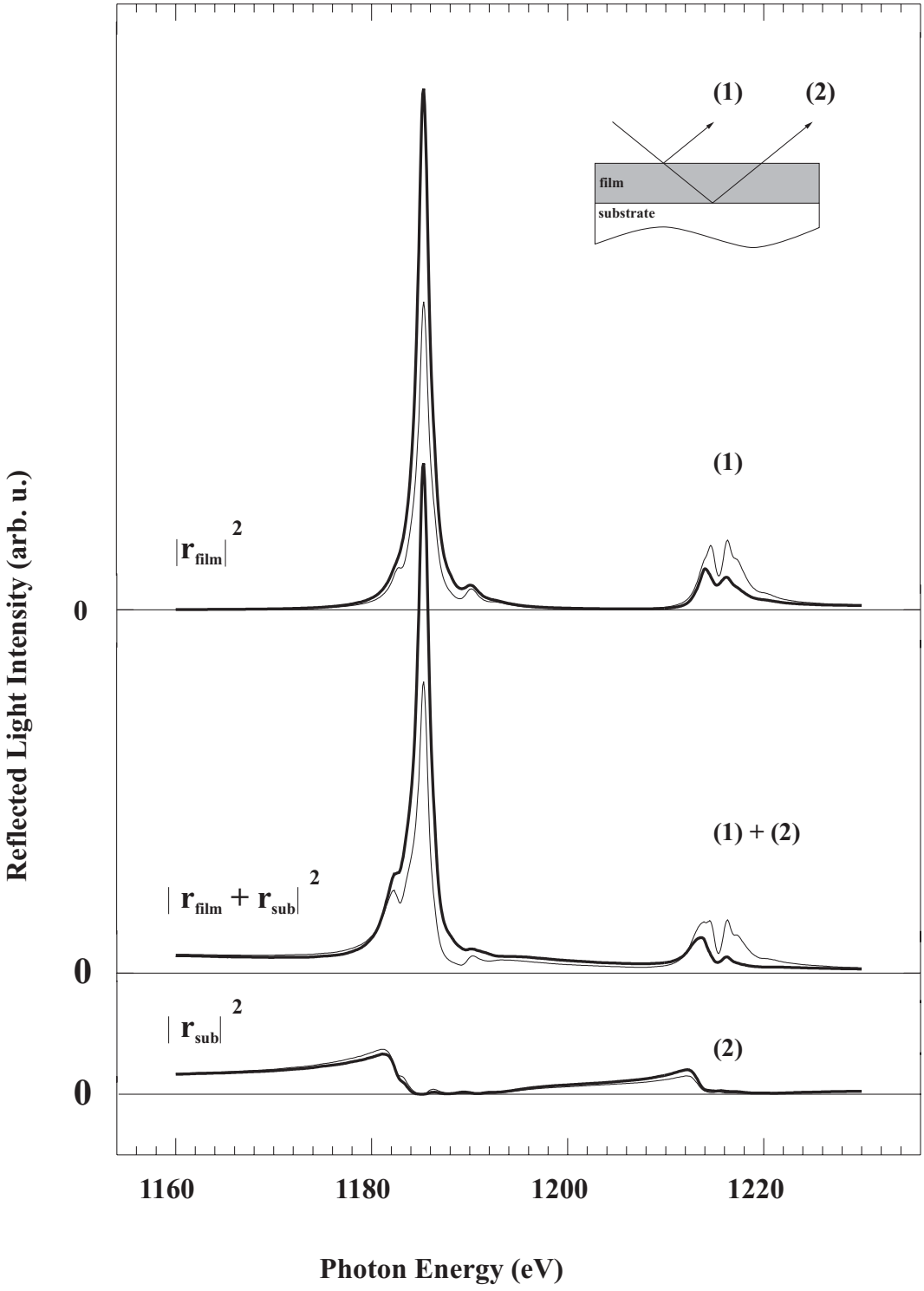

Figure 5.14. Calculated reflectivity of a 10-nm Gd film on a W(110) substrate at 30° of grazing light incidence. The contribution of the film (1) and the substrate (2) are shown separately. r_{film} and r_{sub} denote the amplitudes of the light reflected at the film and at the substrate, respectively.